

RL-TR-95-268
Final Technical Report
January 1996



ADAPTIVE SPACE-TIME PROCESSING FOR AIRBORNE RADAR

The MITRE Corporation

D. Lamensdorf, B.N. Suresh Babu, J.A. Torres,
A.A. Sahraouia, and C.J. Sniezek

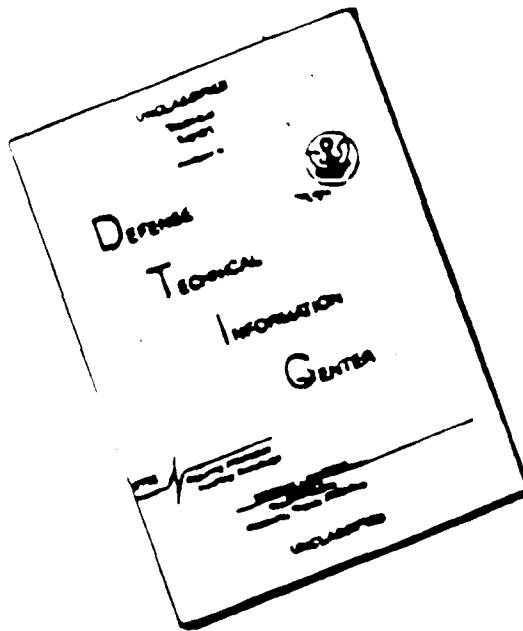
APPROVED FOR PUBLIC RELEASE; DISTRIBUTION UNLIMITED.

19960206 126

Rome Laboratory
Air Force Materiel Command
Rome, New York

DTIC QUALITY INSPECTED 1

DISCLAIMER NOTICE

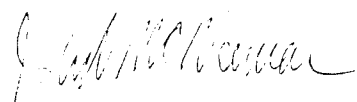


THIS DOCUMENT IS BEST
QUALITY AVAILABLE. THE COPY
FURNISHED TO DTIC CONTAINED
A SIGNIFICANT NUMBER OF
PAGES WHICH DO NOT
REPRODUCE LEGIBLY.

This report has been reviewed by the Rome Laboratory Public Affairs Office (PA) and is releasable to the National Technical Information Service (NTIS). At NTIS, it will be releasable to the general public, including foreign nations.

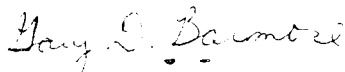
RL-TR-95- 268 has been reviewed and is approved for publication.

APPROVED:



JOHN V. MCNAMARA
Project Engineer

FOR THE COMMANDER:



GARY D. BARMORE, Major, USAF
Deputy Director of Surveillance & Photonics

If your address has changed or if you wish to be removed from the Rome Laboratory mailing list, or if the addressee is no longer employed by your organization, please notify Rome Laboratory/ (OCSA), Rome NY 13441. This will assist us in maintaining a current mailing list.

Do not return copies of this report unless contractual obligations or notices on a specific document require that it be returned.

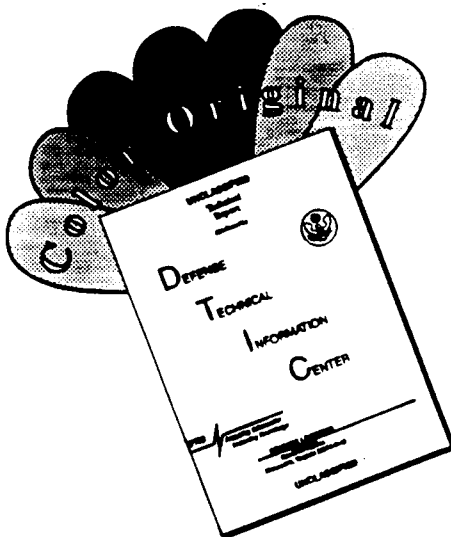
REPORT DOCUMENTATION PAGE

Form Approved
OMB No. 0704-0188

Public reporting burden for this collection of information is estimated to average 1 hour per response, including the time for reviewing instructions, searching existing data sources, gathering and maintaining the data needed, and completing and reviewing the collection of information. Send comments regarding this burden estimate or any other aspect of this collection of information, including suggestions for reducing this burden, to Washington Headquarters Services, Directorate for Information Operations and Reports, 1215 Jefferson Davis Highway, Suite 1204, Arlington, VA 22202-4302, and to the Office of Management and Budget, Paperwork Reduction Project (0704-0188), Washington, DC 20503.

1. AGENCY USE ONLY (Leave Blank)		2. REPORT DATE January 1996	3. REPORT TYPE AND DATES COVERED Final Oct 93 - Sep 94	
4. TITLE AND SUBTITLE ADAPTIVE SPACE-TIME PROCESSING FOR AIRBORNE RADAR			5. FUNDING NUMBERS C - F19628-94-C-0001 PE - 62702F PR - 4506 TA - PR WU - OJ	
6. AUTHOR(S) D. Lamensdorf, B.N. Suresh Babu, J.A. Torres, A.A. Sahraouia, and C.J. Sniezek				
7. PERFORMING ORGANIZATION NAME(S) AND ADDRESS(ES) The MITRE Corporation Burlington Road Bedford MA 01730-0208			8. PERFORMING ORGANIZATION REPORT NUMBER N/A	
9. SPONSORING/MONITORING AGENCY NAME(S) AND ADDRESS(ES) Rome Laboratory/OCSA 26 Electronic Pky Rome NY 13441-4514			10. SPONSORING/MONITORING AGENCY REPORT NUMBER RL-TR-95-268	
11. SUPPLEMENTARY NOTES Rome Laboratory Project Engineer: John V. McNamara/OCSA/(315) 330-4441				
12a. DISTRIBUTION/AVAILABILITY STATEMENT Approved for public release; distribution unlimited.			12b. DISTRIBUTION CODE	
13. ABSTRACT (Maximum 200 words) Significant enhancements have been made to MITRE's computer simulation and processing capability for predicting the performance of airborne phased array radars, and for applying algorithms using space-time adaptive processing (STAP) to suppress interference signals received by these radars. The enhancements include adding elevation degrees of freedom and near-field scattering effects to the steady-state simulation; providing options to transform measured data and to process it in various combinations of spatial and temporal domains; and adding a graphical user interface that is applicable across computer platforms. These enhancements will provide the capability and flexibility needed for the effective application of the simulations to current and planned programs (e.g., Rome Laboratory's Multichannel Airborne Radar Measurements program).				
14. SUBJECT TERMS Airborne phased array radars, Space-time adaptive processing (STAP), Near-field scattering			15. NUMBER OF PAGES 56	
			16. PRICE CODE	
17. SECURITY CLASSIFICATION OF REPORT UNCLASSIFIED	18. SECURITY CLASSIFICATION OF THIS PAGE UNCLASSIFIED	19. SECURITY CLASSIFICATION OF ABSTRACT UNCLASSIFIED	20. LIMITATION OF ABSTRACT UL	

DISCLAIMER NOTICE



THIS DOCUMENT IS BEST QUALITY AVAILABLE. THE COPY FURNISHED TO DTIC CONTAINED A SIGNIFICANT NUMBER OF COLOR PAGES WHICH DO NOT REPRODUCE LEGIBLY ON BLACK AND WHITE MICROFICHE.

TABLE OF CONTENTS

SECTION	PAGE
1 Introduction	1
2 Steady-state Simulation	3
2.1 Elevation Degrees of Freedom	3
2.1.1 Sidelobe Jammer Nulling Example	6
2.1.2 Clutter Suppression Example	6
2.2 Near-Field Scattering	11
2.2.1 Point Scatterer Model	11
2.2.2 Examples of Point Scatterer Model	15
2.2.3 GTD Model	15
2.3 STP Simulation Efficiency	23
3 Finite Sample Processing Capability	25
4 Graphical User Interface	29
5 Demonstration of Steady-State Simulation	31
6 Applications For Simulation And Processing Software	39
7 Conclusion	41
List of References	43
Glossary	45

LIST OF FIGURES

FIGURE		PAGE
1	Jointly-Adaptive Space-Time Processing Architectures	4
2	Flow Chart With Options of Steady-state Simulation	5
3	Performance Measures for Canceling a Sidelobe Jammer With 20 Elevation DOF	7
4	Elevation Receive Antenna Gain Patterns for Canceling a Sidelobe Jammer with 20 Elevation DOF	8
5	Performance Measures for Clutter Cancellation with 8 Elevation DOF	9
6	Elevation Receive Antenna Gain Patterns for Clutter Cancellation with 8 Elevation DOF	10
7	Performance Measures for Clutter Cancellation with 8 Elevation DOF and 4 Pulses	12
8	Elevation Receive Antenna Gain Patterns for Clutter Cancellation with 8 Elevation DOF and 4 Pulses	13
9	Four Simulated Scattering Paths	14
10	Location of Eleven Near-Field Point Scatterers	16
11	Azimuth Receive Antenna Gain Patterns for Canceling a Sidelobe Jammer, without Near-Field Scattering	17
12	Performance Measures for Canceling a Sidelobe Jammer without Near-Field Scattering	18
13	Azimuth Receive Antenna Gain Patterns for Canceling a Sidelobe Jammer, with Near-Field Scattering	19
14	Performance Measures for Canceling a Sidelobe Jammer with Near-Field Scattering	20

FIGURE		PAGE
15	Performance Measures for Canceling Clutter, without Near-Field Scattering	21
16	Performance Measures for Canceling Clutter, with Near-Field Scattering	22
17	Illustrative CPU Run Times for RCF UNIX-Based Computers	24
18	Finite Sample Processing Option	26
19	Signal-To-Interference Ratio Versus Range for Quiescent Processing and Three-Pulse STP for DLR37	27
20	View Simulation Output Data Option	30
21	Examples of Finite Sample Clutter Spectra Created From Simulation with Two Spatial Dimensions of DOF	32
22	MCARM Scenario, Demonstration of Non-Adaptive Performance Using Two Independent Simulations	35
23	MCARM Scenario, Demonstration of Clutter Reduction Using Steady-State STP Simulation	37

SECTION 1

INTRODUCTION

As a result of several recent programs over the past few years, MITRE developed software to predict the performance of airborne phased array radars and algorithms using space-time adaptive processing (STAP) to suppress interference signals received by these radars. There are two types of software capabilities, one is the steady-state performance prediction simulation, which can model the environment of interference signals and the other is finite sample processing, which can process measured or simulated in-phase and quadrature (I & Q) data. These software capabilities have not been adequately evaluated with measured data. Rome Laboratory's (RL's) Multichannel Airborne Radar Measurements (MCARM) program is currently developing a testbed that will obtain this type of data. The objective of this project is to enhance MITRE's simulation and processing capability to develop benchmarks for the RL testbed for determining its potential performance, and to process and evaluate the measured data that will be obtained from this testbed in FY95.

The project can be described by four overall tasks. Two tasks cover upgrades to each of the software capabilities. One is the application of an improved graphics interface, and one is a demonstration of the steady-state simulation plus recommendations for their application.

- Several enhancements have been made to the capability of the simulation model that predicts the steady-state performance. Elevation degrees of freedom (DOF) and a model for multiple point near-field scatterers has been added. Also, the outputs of a simulation code based upon geometric optics and diffraction that provides more detailed models of the interaction with aircraft scatterers can be inserted directly into the simulation. The simulation has been reorganized to run more efficiently.
- The finite sample processing software can now apply spatial and/or temporal preprocessing transformations to a cube of received I & Q data. The covariance matrix used to calculate the adapted weights is obtained from the transformed data.
- A mouse driven front-end with menus has been applied to the simulation and processing software. A graphical user interface (GUI) with several plotting package options has been provided for showing the input files and the output performance measures. Most of these have cross-platform capability.
- The simulation has been demonstrated for scenarios based upon the planned MCARM experiments. Future applications of these simulations have been recommended based upon these experiments, potential Airborne Warning and Control System (AWACS) applications, the ARPA (Advanced Research Projects Agency) mountain top data reduction, and the proposed Bistatic Adjunct Surveillance System (BASS).

SECTION 2

STEADY-STATE SIMULATION

MITRE's Advanced Airborne Radar Simulation is based upon the STAP architecture shown in Figure 1 [1-4]. Tapped delay lines are placed at the output of each array output, with the taps spaced by one pulse repetition interval (PRI). The adapted weights are obtained by multiplying the inverse of the covariance matrix created from the received signals (interference-plus-target-plus-noise signals) at each of the tap outputs with a steering vector. Each weight is applied to the appropriate PRI tap (i.e., pulse), and the weighted pulse outputs are coherently summed to provide the adapted output signal. The number of DOF is the number of pulses times the number of array outputs (elements, beams, or subarrays). When the number of pulses used in the STAP filter is less than the number of PRI outputs to be coherently processed, Doppler processing following the STAP filter summation provides further coherent gain for the target signal. The STAP performance (e.g., signal-to-interference ratio (SIR)) can be measured at the output of the summation and at any Doppler filter output. Additional temporal taps spaced by a sampling interval that is less than the length of a compressed pulse represents another dimension of DOF that can be applied to the output of each PRI tap for suppressing multipath and for channel mismatch [4]. The individual steady-state covariance matrices for the received clutter signals, jammer signals, and thermal noise are calculated based upon their modeled spatial and temporal correlation properties as affected by the platform velocity and crab angle, internal clutter motion, signal bandwidth, and the match of the output channels. Additional insight into the adapted performance is provided by calculating the eigenspectra of the interference covariance matrix and the adapted antenna gain patterns. Figure 2 is a global flow chart showing the options of the steady-state simulation with the shaded portions identifying the new capabilities that have been provided.

2.1 ELEVATION DOF

The Advanced Airborne Radar Simulation employs a planar array with a specified aperture weighting and with the antenna element gain pattern. Previously, the simulation characterized each column of the planar array on receive as a single non-adapted elevation subarray. The effects of azimuth spatial DOF on the performance of STAP can be evaluated by adaptively processing the outputs of these receive azimuth subarrays. However, for medium- and high-pulse repetition frequency (PRF) waveforms, the long-range target and short-range clutter may compete with each other because of range folding. For these waveforms, the space-time processing (STP) architecture may require additional spatial DOF in elevation to reduce the contributions of the short-range clutter as discussed below.

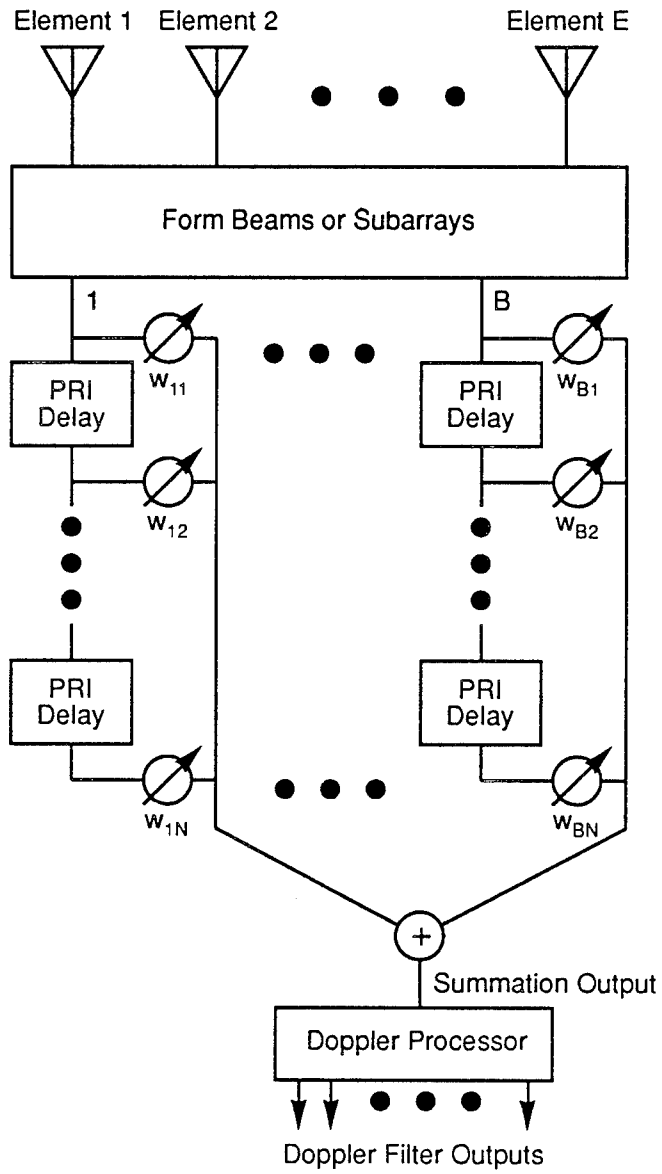


Figure 1. Jointly-Adaptive Space-Time Processing Architectures

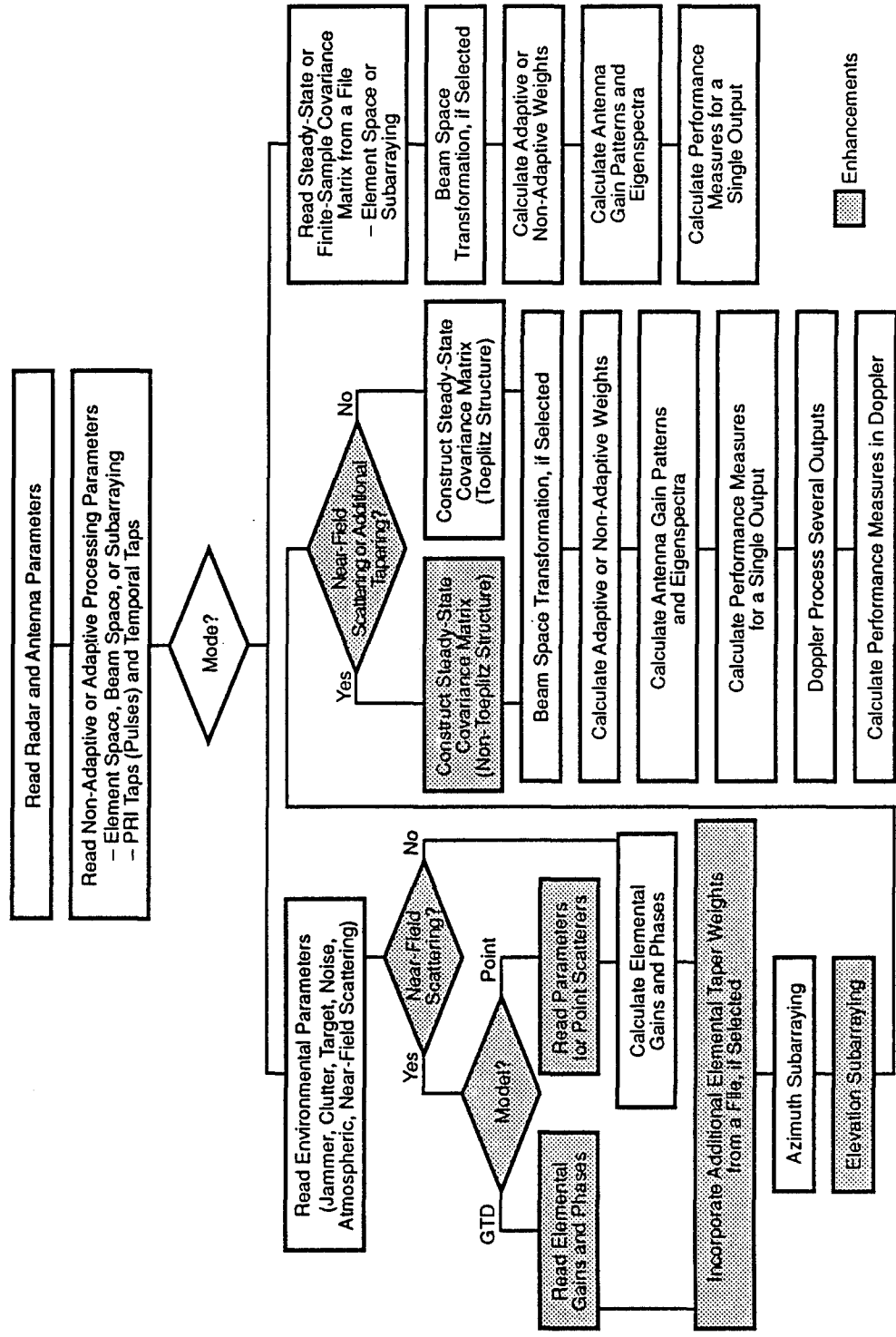


Figure 2. Flow Chart With Options of Steady State Simulation

The simulation has been modified to allow the calculation an equal number of multiple non-adapted subarrays in elevation for each array column or azimuth subarray. Earlier the simulation had 52 subroutines. Fifteen subroutines were modified to incorporate this adaptive elevation DOF capability.

Two examples illustrate the elevation DOF feature of the simulation. First, we validate the program using a horizontal linear array with a single sidelobe jammer in a clutter-free environment. We then rotated the array by 90 degrees and placed the single jammer at the same angular location in elevation. The jammer-plus-noise-to-noise ratio (JNR) results from the two programs were identical when using the modified simulation. Second, we illustrate how elevation DOF can be used to mitigate short- and long-range clutter competing with a long-range target. Although the spatial elevation DOF alone can mitigate short-range clutter, additional temporal DOF are required to cancel long-range clutter while maintaining the mainbeam and not canceling the target.

2.1.1 Sidelobe Jammer Nulling Example

In this example, we chose a horizontal 20-element linear array electronically scanned in azimuth to -10 degrees (relative to broadside) and a sidelobe jammer located in azimuth at -32 degrees (relative to broadside). Using the previous steady-state version of the simulation, the quiescent JNR was 44 dB, and the adapted JNR using element space processing (i.e., 20 azimuth DOF) was 8.2 dB. Note that the jammer was not completely canceled due to a specified cancellation ratio of 55 dB. Next, a vertical 20-element linear array (i.e., 20 elevation DOF) electronically scanned in elevation to 10 degrees was used to cancel a sidelobe jammer at 32 degrees in elevation. Figure 3 shows the quiescent and adapted JNR using the modified simulation. Figure 4 shows the quiescent and adapted elevation receive antenna gain patterns, illustrating that there is an adapted null at 32 degrees used to cancel the sidelobe jammer. The performance measures and patterns were identical for the horizontal and vertical array configurations demonstrating the successful implementation of two dimensions of spatial DOF in the simulation.

2.1.2 Clutter Suppression Example

This example illustrates how elevation DOF can adaptively cancel short- and long-range clutter competing with a long-range target. For this example we use a 30 x 8 planar array electronically scanned in elevation to 2.8 degrees. The PRF of the radar waveform is 1400 Hz, which causes an additional three range ambiguities at elevation angles of 3.1, 4.9, and 75.4 degrees, respectively. Figure 5 shows the performance measures when eight elevation DOF are used to adaptively cancel the clutter. The clutter-plus-noise-to-noise ratio (CNR) is reduced from 60 to 0.3 dB. However, there is also target cancellation, as indicated by the significant loss in signal-to-noise ratio (SNR) and small improvement in SIR. The quiescent and adapted elevation receive antenna gain patterns shows the cancellation of both the target and clutter. Figure 6 illustrates that an adaptive null in the elevation gain pattern at 75.4 degrees cancels the short-range clutter.

Performance * Measures (in dB)	Adaptive	Quiescent
$\left(\frac{J+N}{N}\right)$	8.21	44.02
$\left(\frac{S}{I}\right)$	28.87	-6.91
$\left(\frac{S}{N}\right)$	37.09	37.11

* $\left(\frac{J+N}{N}\right)$ = jammer-plus-noise-to-noise ratio

$\left(\frac{S}{I}\right)$ = signal-to-interference ratio

$\left(\frac{S}{N}\right)$ = signal-to-noise ratio

Figure 3. Performance Measures for Canceling a Sidelobe Jammer With 20 Elevation DOF

Number of Antenna Columns = 1
Number of Antenna Rows = 20
Frequency = L-Band
Elevation Weighting = 30 dB Taylor, $\bar{N} = 5$
Elevation Electronic Scan Angle = 10 Degrees

Radar Bandwidth = 1.0E06 Hz
Jammer Model = Wideband
Jammer Elevation Angle = 32 Degrees
Cancellation Ratio = 55 dB
Number of Pulses Processed = 1

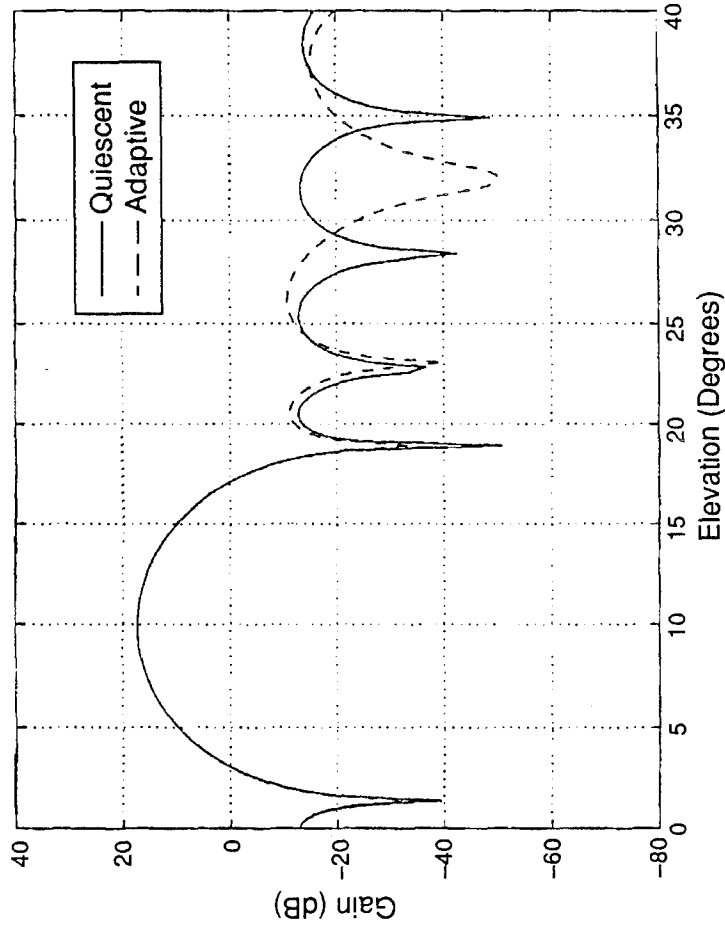


Figure 4. Elevation Receive Antenna Gain Patterns for Canceling a Sidelobe
Jammer with 20 Elevation DOF

Performance * Measures (in dB)	Adaptive	Quiescent
$\left(\frac{C+N}{N}\right)$	0.34	60.10
$\left(\frac{S}{I}\right)$	-40.46	-54.37
$\left(\frac{S}{N}\right)$	-40.12	5.74

* $\left(\frac{C+N}{N}\right)$ = clutter-plus-noise-to-noise ratio

$\left(\frac{S}{I}\right)$ = signal-to-interference ratio

$\left(\frac{S}{N}\right)$ = signal-to-noise ratio

Figure 5. Performance Measures for Clutter Cancellation with 8 Elevation DOF

Number of Antenna Columns = 30
 Number of Antenna Rows = 8
 Frequency = L-Band
 PRF = 1400 Hz
 Azimuth Weighting = 30 dB Taylor, $\bar{N} = 5$
 Elevation Weighting = 30 dB Taylor, $\bar{N} = 5$
 Elevation Electronic Scan Angle = 2.8 Degrees
 Radar Bandwidth = 1.0E06 Hz
 Clutter Model = Constant Gamma (-9 dB)
 Number of Range Ambiguities = 3
 Number of Receive Azimuth Subarrays = 1
 Number of Pulses Processed = 1

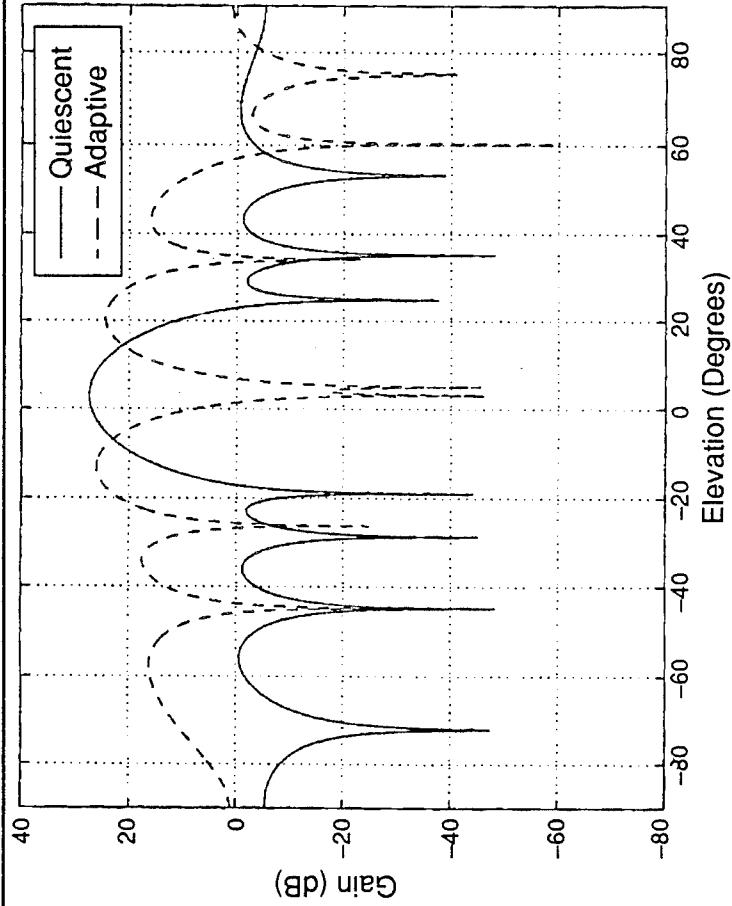


Figure 6. Elevation Receive Antenna Gain Patterns for Clutter Cancellation with 8 Elevation DOF

However, there are adaptive nulls in the mainlobe corresponding to the elevation angle locations of the long-range clutter (which includes the elevation location of the target).

Temporal DOF (i.e., pulses) can adaptively discriminate a moving target from the long-range clutter in the main beam. Figure 7 shows the performance measures using 32 DOF where four temporal and eight elevation DOF are used simultaneously to cancel the clutter. Eigenvalue compensation was applied to minimize antenna pattern distortion [3]. The CNR is reduced from 60.0 to 6.5 dB, while the SNR is increased from 5.7 to 10.7 dB, resulting in a significant improvement in SIR from -54.4 to 4.1 dB. Figure 8 illustrates the elevation receive antenna gain pattern evaluated at the target Doppler (i.e., half the blind speed).

2.2 NEAR-FIELD SCATTERING

Near-field scattering by the radar's platform can degrade the free-space pattern of the antenna by redirecting energy from the sidelobes into the mainbeam, thereby degrading the radars performance. STP has been shown to be an effective technique for mitigating near-field scattering [6]. For each clutter scatterer, the software calculates an entry of the steady-state covariance matrix based on the radar range equation, the free-space transmit gain pattern of the array, and the linear phase terms due to the clutter's spatial (i.e., element-to-element) and temporal (i.e., tap-to-tap and pulse-to-pulse) correlation properties. In the absence of near-field scattering, the clutter steady-state covariance matrix is spatially and temporally stationary, and is constructed by calculating only a single row of entries and exploiting its Toeplitz structure. However, one of the critical factors that can limit the performance of STAP is the near-field scattering effects due to the antenna-aircraft interactions. The modifications to include the scattering effects from near-field obstacles in the simulation's steady-state mode are described below.

2.2.1 Point Scatterer Model

The effects of multipath caused by point scatterers in the near-field of the array antenna can be described by the sum of four scattering paths as illustrated in Figure 9. The direct transmit and receive path between the array and a clutter patch in the far field of the array on the ground is shown in Figure 9a. Near-field scattering creates three additional paths. One bounce path on receive as in Figure 9b requires augmenting the steady-state covariance matrix calculation with additional non-linear phase terms due the nonstationary spatial correlation properties of the received clutter. One bounce path on transmit as in Figure 9c requires the calculation of the far-field transmit gain pattern in the presence of the near-field point scatterers. The two-bounce path in Figure 9d is a composite of one bounce path on transmit and one on receive. These three added bounce paths cause the steady-state covariance matrix for the received clutter to be non-Toeplitz, where all entries of the matrix need to be calculated explicitly. Therefore, this modification can significantly increase the computational complexity and run time of the simulation.

Performance * Measures (in dB)	Adaptive	Quiescent
$\left(\frac{C+N}{N}\right)$	6.51	60.10
$\left(\frac{S}{I}\right)$	4.14	-54.37
$\left(\frac{S}{N}\right)$	10.65	5.74

* $\left(\frac{C+N}{N}\right)$ = clutter-plus-noise-to-noise ratio

$\left(\frac{S}{I}\right)$ = signal-to-interference ratio

$\left(\frac{S}{N}\right)$ = signal-to-noise ratio

Figure 7. Performance Measures for Clutter Cancellation with 8 Elevation DOF and 4 Pulses

Number of Antenna Columns = 30 Elevation Electronic Scan Angle = 2.8 Degrees
 Number of Antenna Rows = 8 Radar Bandwidth = 1.0E06 Hz
 Frequency = L-Band Clutter Model = Constant Gamma (-9 dB)
 PRF = 1400 Hz Number of Range Ambiguities = 3
 Azimuth Weighting = 30 dB Taylor, $\bar{N} = 5$ Number of Receive Azimuth Subarrays = 1
 Elevation Weighting = 30 dB Taylor, $\bar{N} = 5$ Number of Pulses Processed = 4

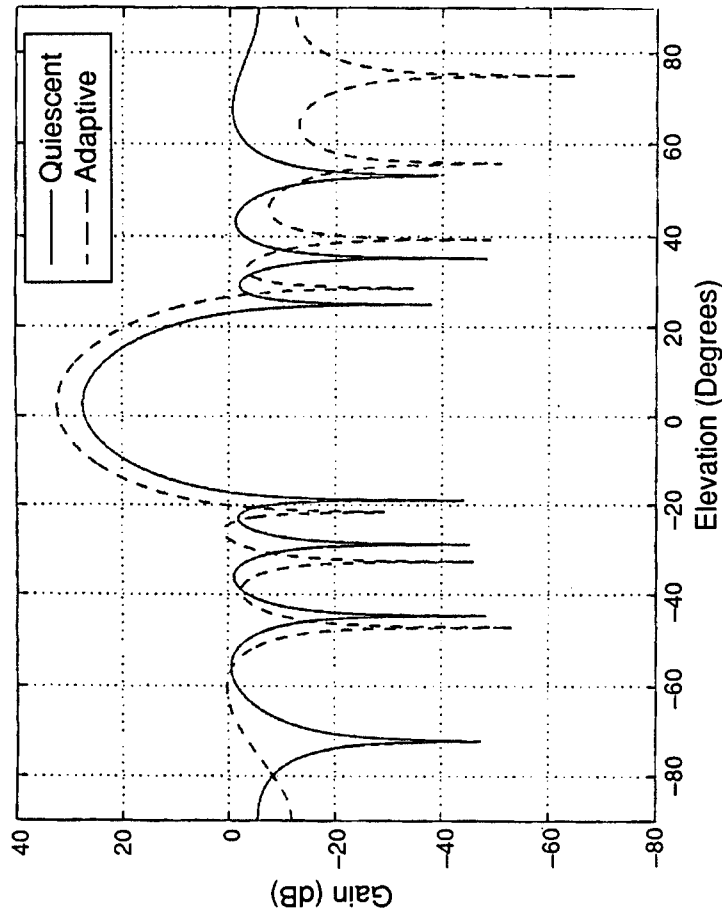


Figure 8. Elevation Receive Antenna Gain Patterns for Clutter Cancellation with 8 Elevation DOF and 4 Pulses

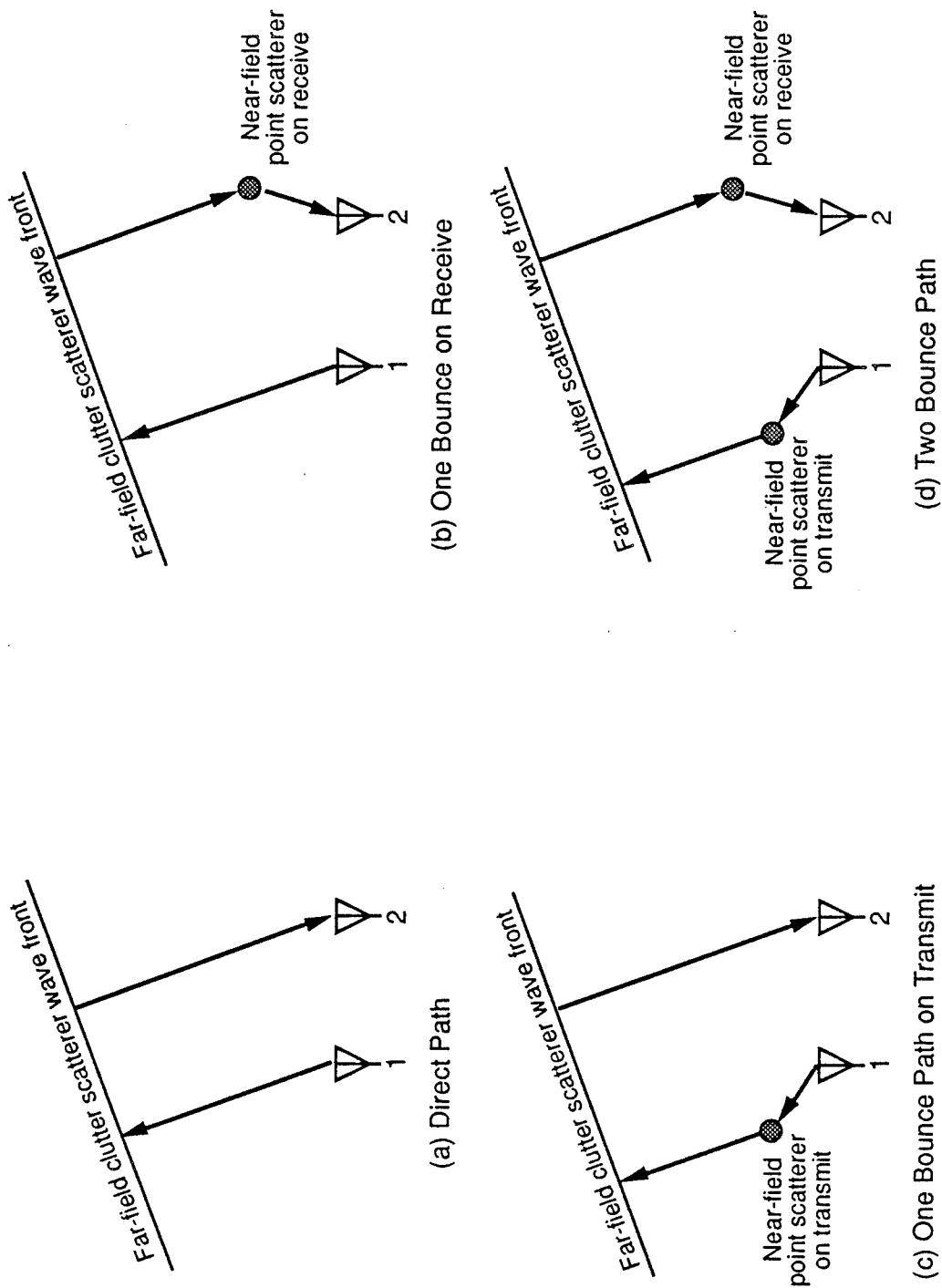


Figure 9. Four Simulated Scattering Paths

2.2.2 Examples of Point Scatterer Model

Two examples are presented to illustrate the near-field point scattering model of the simulation. First is the effect of near-field scattering on the cancellation of a single sidelobe jammer and second is its effect on clutter cancellation.

A 16-element horizontal linear array was simulated, with the antenna-platform interactions represented by a line of eleven closely spaced point scatterers (each with a bistatic cross section of 2 m^2), as shown in Figure 10. The array is collinear with the x-axis and centered about the origin, and the platform heading is in the positive x-direction. The single sidelobe jammer is located at -43 degrees in azimuth. Figure 11 shows the quiescent and adapted receive antenna gain patterns without near-field scattering. Figure 11 shows the quiescent and adapted performance measures in the absence of near-field scattering. The jammer was not completely canceled (i.e., adapted JNR equal 2.9 dB) due to the channel matching, cancellation ratio of 50 dB as shown in Figure 12. In comparison, Figure 13 shows the quiescent and adapted patterns in the presence of the near-field point scatterers. The quiescent gain in the azimuth direction of the jammer increased the JNR by almost 13 dB , as shown in Figure 14. The near-field scattering and channel mismatch effects increased the adapted JNR to 6.3 dB . However, if the bistatic cross section of each of the near-field scatterers is reduced, the adapted performance approaches the level achieved without near-field scattering.

The effect of the line of point near-field scatterers on clutter suppression was illustrated with a horizontal linear array of columns. Figure 15 shows the adapted SIR without near-field scattering for a varying number of spatial DOF or columns and temporal DOF or pulses. The adapted SIR is normalized by the adapted SIR obtained in the noise-only case resulting in a maximum achievable value of 0 dB . From Figure 15, for example, canceling the clutter with an internal motion of 0.1 m/s and adapted SIR of -3 dB requires eight elements and three pulses. Figure 16 shows the adapted SIR for the same array with the line of eleven near-field point scatterers. In order to achieve an adapted SIR of less than 3 dB with eight to twelve columns now requires four pulses and there is a considerable degradation with only four columns.

2.2.3 Geometric Theory of Diffraction (GTD) Model

The second modification uses a simulation that models the electromagnetic interaction between an antenna and its platform (e.g., the airplane on which it is mounted). The Numerical Electromagnetics Code-Basic Scattering Code (NECBSC), a simulation that is based upon geometric optics and the GTD. It determines the complex amplitude and phase information at each far-field point (corresponding to a clutter scatterer location) due to each transmit antenna element in the presence of a model of the aircraft structure. This simulation was developed by Ohio State University to model interactions between antennas and their platforms [7]. The signal at each of the array outputs obtained from this GTD-based

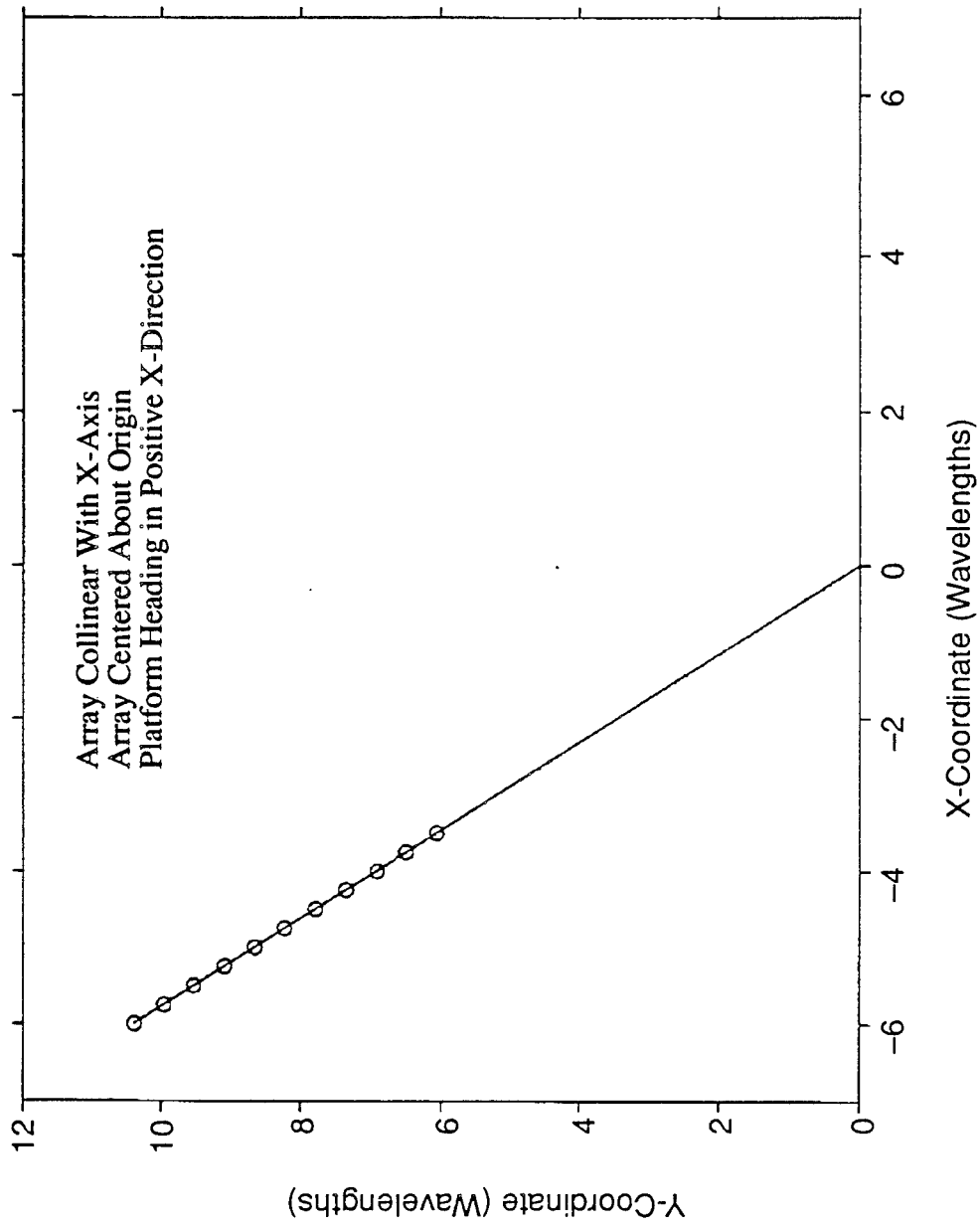


Figure 10. Location of Eleven Near-Field Point Scatterers

Number of Antenna Columns = 16
Number of Antenna Rows = 1
Frequency = L-Band
Azimuth Weighting = Uniform
Azimuth Electronic Scan Angle = 0 Degrees
Radar Bandwidth = 1.0E06 Hz

Jammer Model = Wideband
Jammer Azimuth Angle = -43 Degrees
Cancellation Ratio = 50 dB
Number of Pulses Processed = 1
Number of Near-Field Point Scatterers = 0

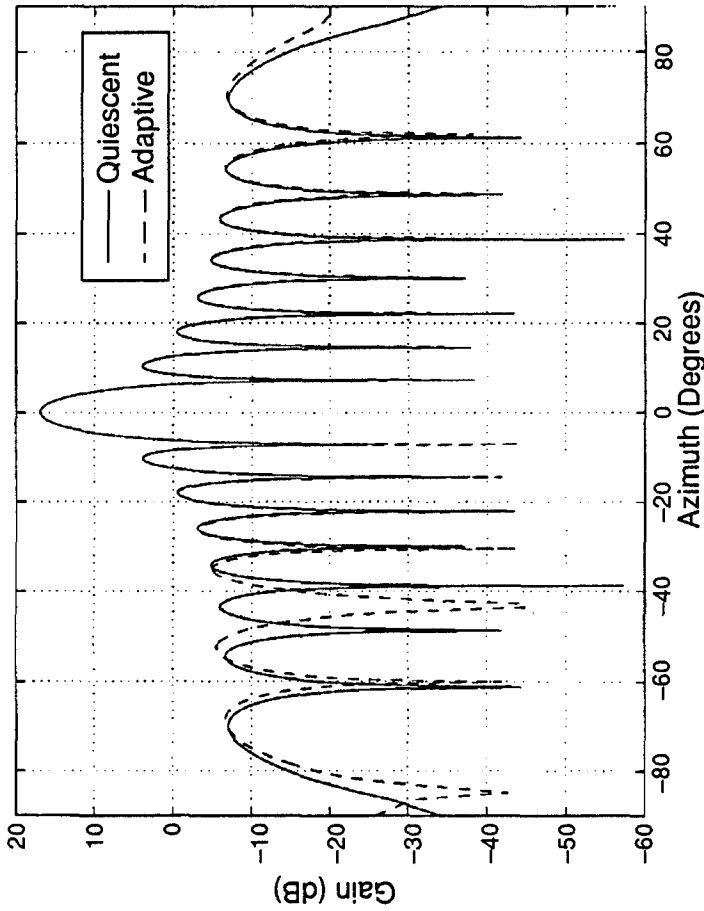


Figure 11. Azimuth Receive Antenna Gain Patterns for Cancelling a Sidelobe Jammer, Without Near-Field Scattering

Performance * Measures (in dB)	Adaptive	Quiescent
$\left(\frac{J+N}{N}\right)$	2.92	38.80
$\left(\frac{S}{I}\right)$	21.58	-14.28
$\left(\frac{S}{N}\right)$	24.50	24.52

* $\left(\frac{J+N}{N}\right)$ = jammer-plus-noise-to-noise ratio

$\left(\frac{S}{I}\right)$ = signal-to-interference ratio

$\left(\frac{S}{N}\right)$ = signal-to-noise ratio

Figure 12. Performance Measures for Cancelling a Sidelobe Jammer Without Near-Field Scattering

Number of Antenna Columns = 16
Number of Antenna Rows = 1
Frequency = L-Band
Azimuth Weighting = Uniform
Azimuth Electronic Scan Angle = 0 Degrees
Radar Bandwidth = 1.0E06 Hz

Jammer Model = Wideband
Jammer Azimuth Angle = -4.3 Degrees
Cancellation Ratio = 50 dB
Number of Pulses Processed = 1
Number of Near-Field Point Scatterers = 11
Bistatic Cross-Section = 2.0 m²

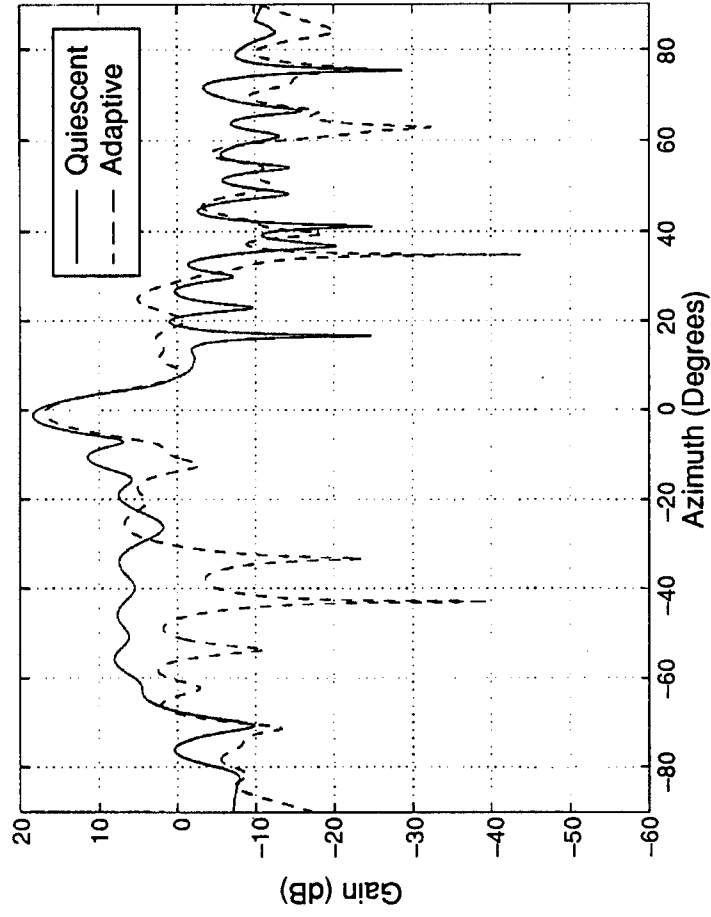


Figure 13. Azimuth Receive Antenna Gain Patterns for Cancelling a Sidelobe Jammer, With Near-Field Scattering

Performance * Measures (in dB)	Adaptive	Quiescent
$\left(\frac{J+N}{N}\right)$	6.35	51.61
$\left(\frac{S}{I}\right)$	16.97	-27.09
$\left(\frac{S}{N}\right)$	23.31	24.52

* $\left(\frac{J+N}{N}\right)$ = jammer-plus-noise-to-noise ratio

$\left(\frac{S}{I}\right)$ = signal-to-interference ratio

$\left(\frac{S}{N}\right)$ = signal-to-noise ratio

Figure 14. Performance Measures for Cancelling a Sidelobe Jammer With Near-Field Scattering

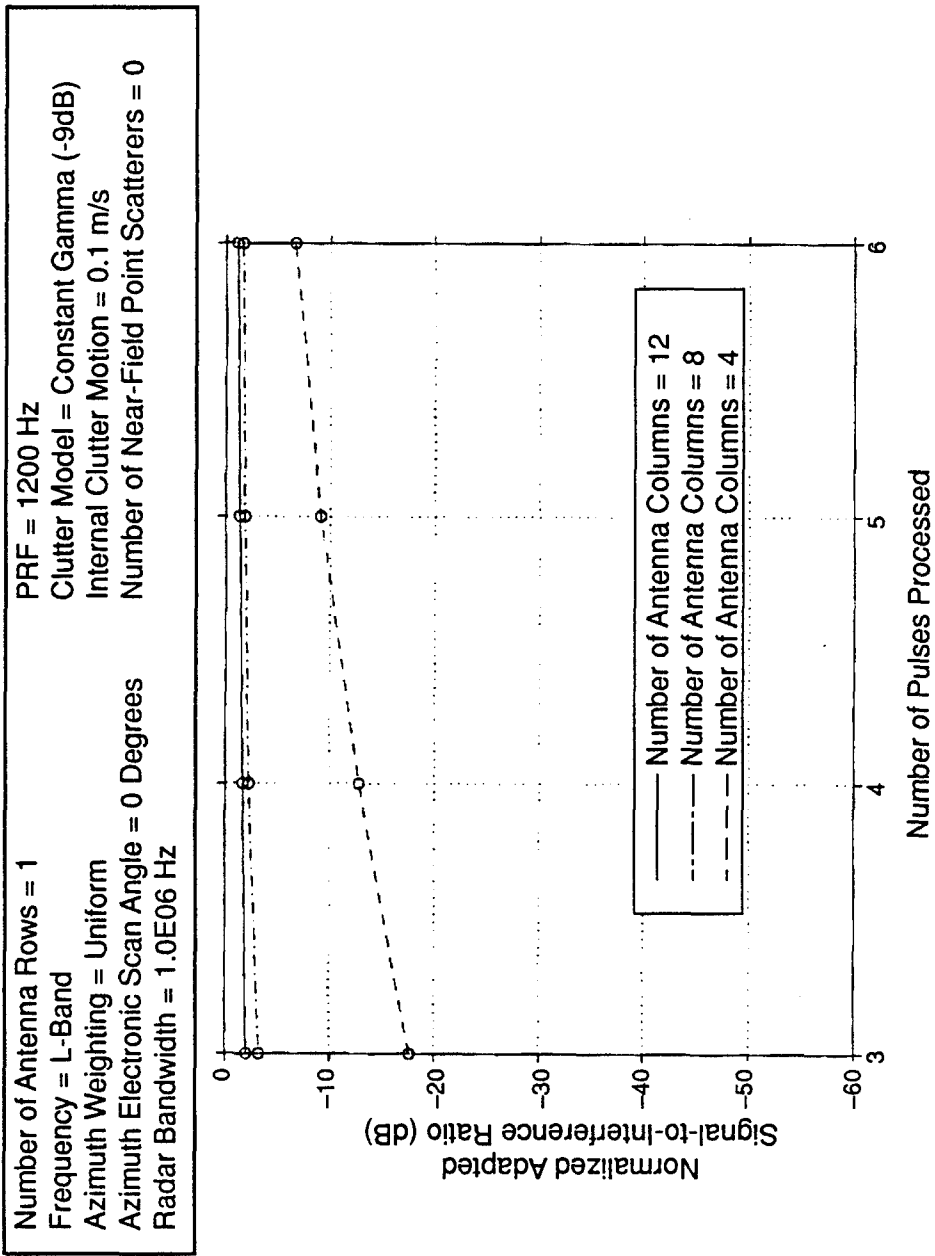


Figure 15. Performance Measures for Cancelling Clutter, Without Near-Field Scattering

Number of Antenna Rows = 1
 Frequency = L-Band
 Azimuth Weighting = Uniform
 Azimuth Electronic Scan Angle = 0 Degrees
 Radar Bandwidth = 1.0E06 Hz
 PRF = 1200 Hz
 Clutter Model = Constant Gamma (-9 dB)
 Internal Clutter Motion = 0.1 m/s
 Number of Near-Field Point Scatterers = 11
 Bistatic Cross-Section = 2.0 m²

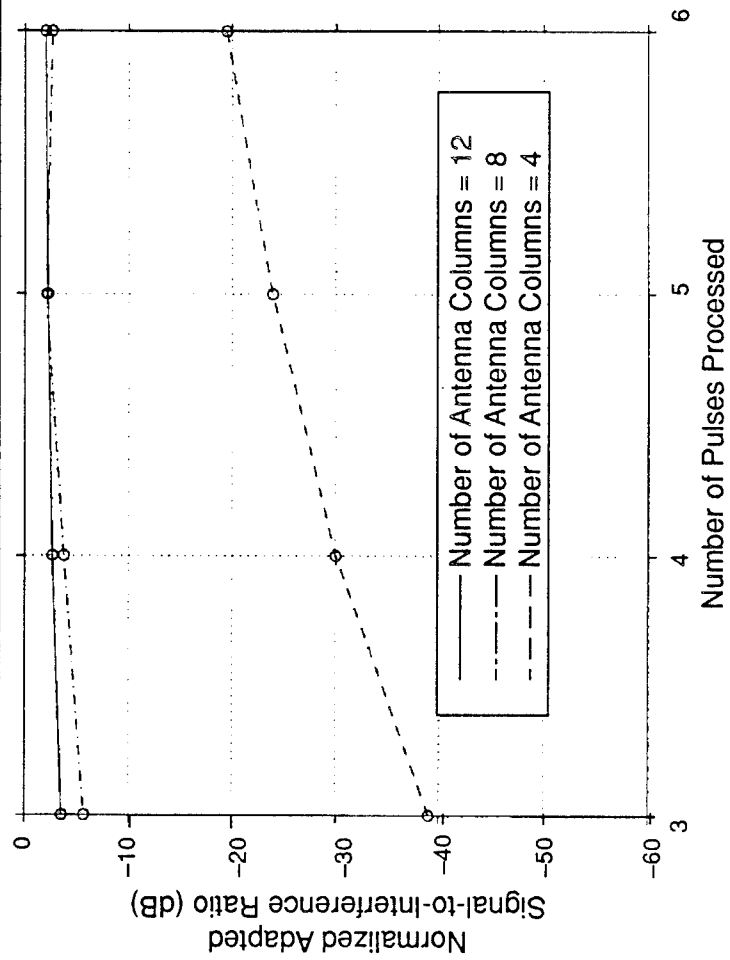


Figure 16. Performance Measures for Cancelling Clutter, With Near-Field Scattering

simulation is stored on an output file that can be read into the steady state STAP simulation to construct the clutter steady-state covariance matrix [8]. The STAP performance predicted using this modification is based upon a more accurate model of both the near-field scatterer and the electromagnetic scattering phenomenology in comparison with the point scatterer model. However, this is provided at the expense of a significant increase in computation time because of this GTD simulation, particularly for a large array antenna.

2.3 STP SIMULATION EFFICIENCY

In the process of enhancing the steady-state STAP simulation to provide the new capabilities that have been described, the code has been reorganized. Each of the processing options, configurations for each dimension of DOF, interference signal scenarios (jammers and clutter), plus various aircraft-antenna interactions are described by separate callable subroutines. This enables the simulation to be readily applied to many radar scenarios. It has also enabled the CPU running time for the code to be sped up, which can be significant for large arrays. An example of this improved CPU efficiency is shown in Figure 17.

Number of Antenna Rows (NUMELEV) = 8
 Number of Clutter Scatterers (NCL) = 181
 Number of Jammers (NESI) = 4
 Adaptive Processing (IADAPT = 1)
 Subarray Space Architecture (IELEM = 1)
 Number of Elevation Subarrays (NSUB_EL) = 1
 Number of Pulses Processed (NP) = 2
 Number of Frequency Components (NFR) = 1
 Number of Range Rings = 1
 No MTI Preprocessing (IUSMTI = 0)
 No Antenna Pattern Calculation (IPLOTP = 0)
 No Eigenvalue Compensation (ICORR = 0)
 No Eigenvalue Calculation (IPRNTEIG = 0)
 Number of Doppler Filters (NDOP) = 50
 Number of Coherently Integrated Outputs (NCI) = 16

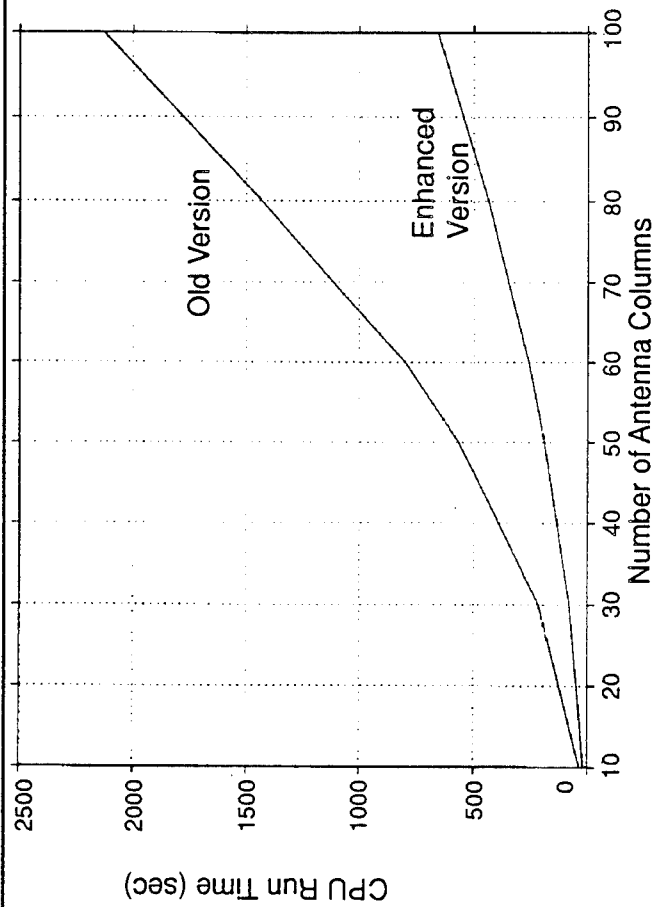


Figure 17. Illustrative CPU Run Times for RCF UNIX-Based Computers

SECTION 3

FINITE SAMPLE PROCESSING CAPABILITY

The data received from a pulse-Doppler radar is represented by a non-stationary train of pulses. For the application of STAP, these pulses must be recorded coherently (e.g., as I & Q data for each pulse). An estimated covariance matrix is created by averaging the covariances over a finite number of space (adjacent range cells) and time (pulses) samples from the data [8]. (This differs from the steady-state simulation where the covariance matrix represents an average based upon an infinite number of samples from each clutter cell.) Adapted weights are obtained by multiplying the inverse of this estimated covariance matrix by the steering vector. These weights can now be applied to the data samples corresponding to the ranges and pulses over which the weights were averaged.

The finite sample processing code that was developed earlier [8] has been modified to provide more flexible processing options. A flow chart of the modified code is shown in Figure 18. It begins with an input consisting of a finite train of I & Q data samples that are the outputs received by the array antenna. These received data samples can be obtained from measured data or from a simulation to create the finite train of received data samples.

A cube of data is created from this finite number of data samples. The axes of the cube are the spatial DOF (horizontal and vertical element outputs of the array), temporal DOF (pulses), and the contiguous range cell samples. Options for preprocessing transformations of the data are then provided: Spatial transformations from element space to either beam-space or subarray space and temporal transformations from pulses to Doppler frequency.

The inverse of the estimated covariance matrix obtained from all or a subset of the finite sample data cube is multiplied by the appropriate steering vector to create the adaptive weights. These weights are then applied to the data cube to obtain the processed output signal. The adaptive processing options include N-pulse STAP followed by Doppler processing (where N is less than the total number of coherent pulses recorded) and higher-order Doppler frequency-factored processing [9]. The available output performance measures are the interference signal level and the SIR versus range or Doppler frequency. To illustrate this finite sample processing capability, a data file from the Naval Research Laboratory eight-element airborne UHF array was processed. The SIR versus range performance with no processing and with three-pulse STP is shown in Figure 19. For this example, the target signal at each range is made proportional to the steering vector and is not a function of elevation angle. In general, to calculate the SIR when the target signal is not already in the data (e.g., to insert a target signal) will require the development of a simulated target signal as a function of elevation gain pattern and Doppler frequency.

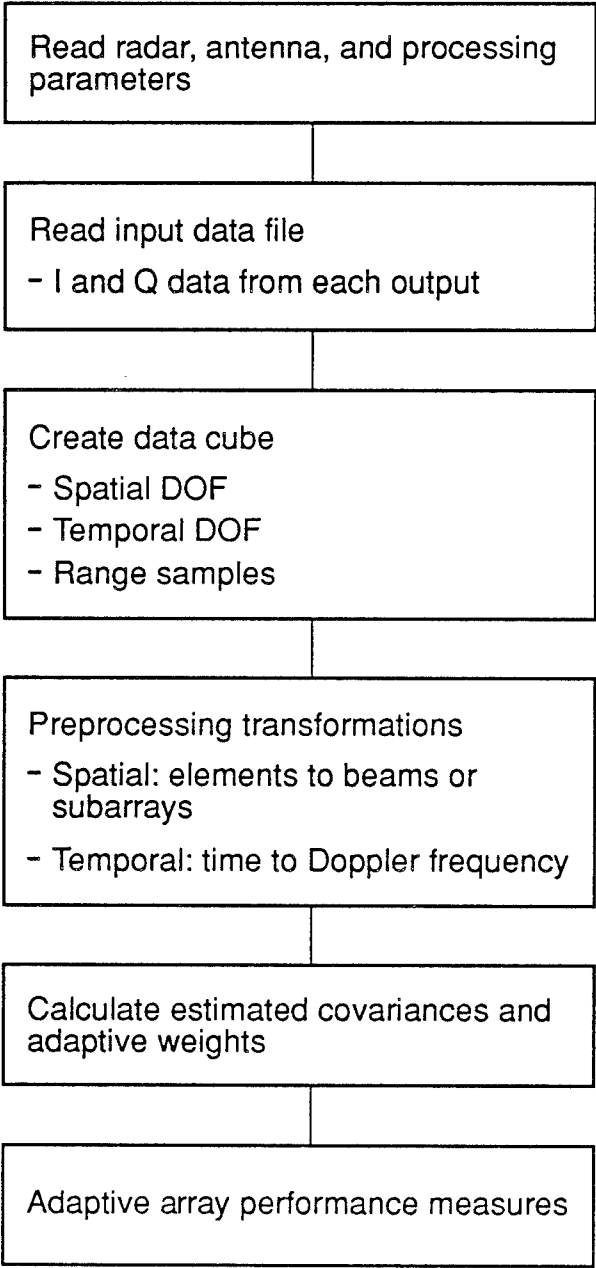


Figure 18. Finite Sample Processing Option

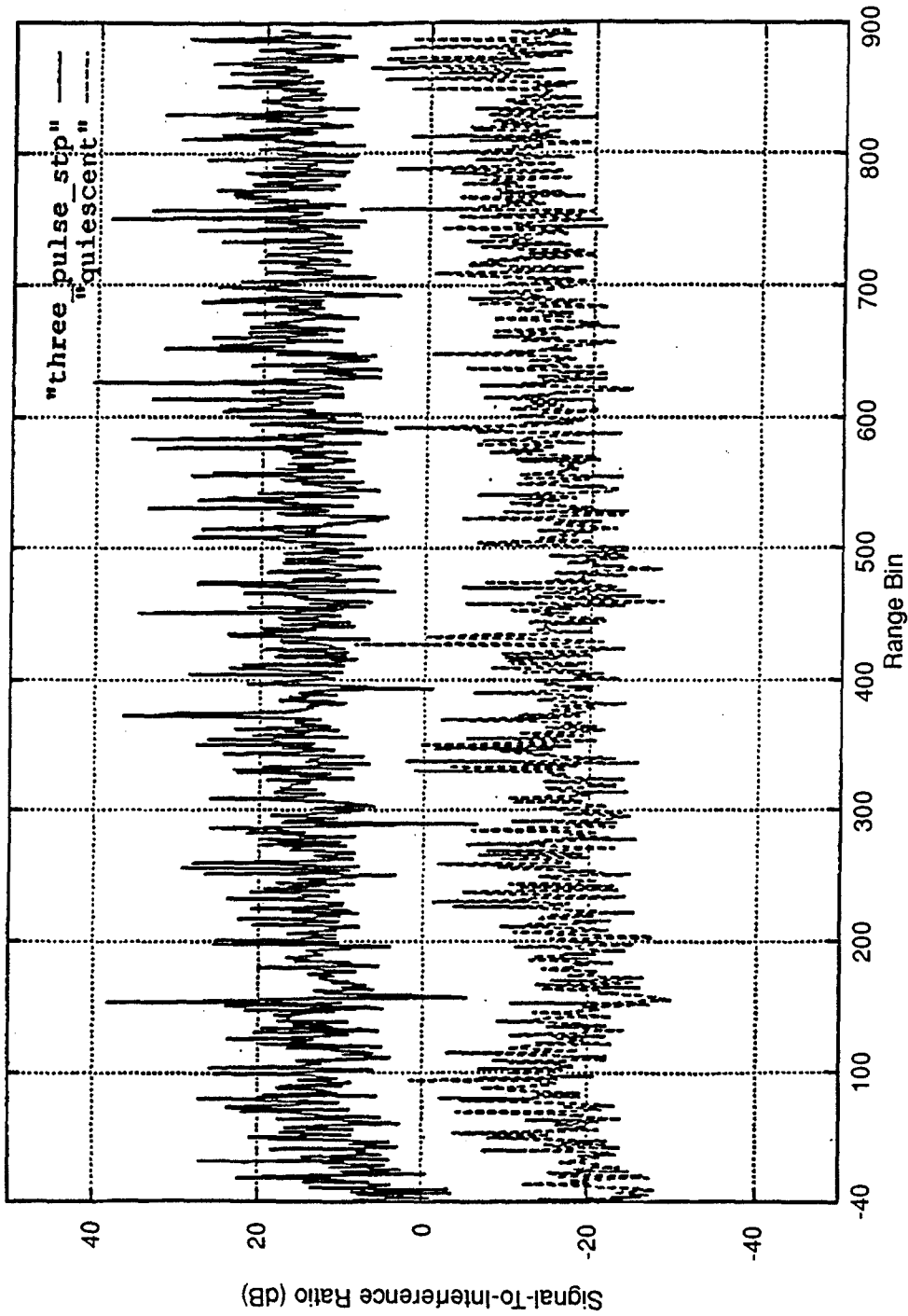


Figure 19. SIR Versus Range for Quiescent Processing and Three-Pulse STP for DLR37

SECTION 4

GRAPHICAL USER INTERFACE

A GUI has been provided as an intuitive means for running the software and displaying its output [10]. Interaction using the interface to the software is mouse-based with pull-down menus describing output options. The GUI prompts the user for an interactive editing and verification of an input file, runs the software, and then offers several options for viewing and storing the output. This is illustrated by the pull down menu in Figure 20 for providing the options for viewing the output data.

The interface is written in a relatively new interpreted scripting language developed by J. Ousterhout at U. C. Berkeley called Tool Command Language and Toolkit (Tcl and Tk). This language was chosen for several reasons, including its cross-platform functionality and the short time and simplicity with which applications can be developed and modified using it.

The cross-platform functionality of the GUI and the plotting software, GNUPLOT, (a freeware package developed at Dartmouth) that has been implemented with it was important in their selection since the simulation runs on both VMS and UNIX platforms. Tcl uses the same interpretation method for both types of operating systems. Also, since the script is easily modifiable to accommodate any plotting software package that can be loaded as a series of plotting instructions at the command line, other software for creating plots can also be used for specific platforms for which they are available, such as MATLAB.

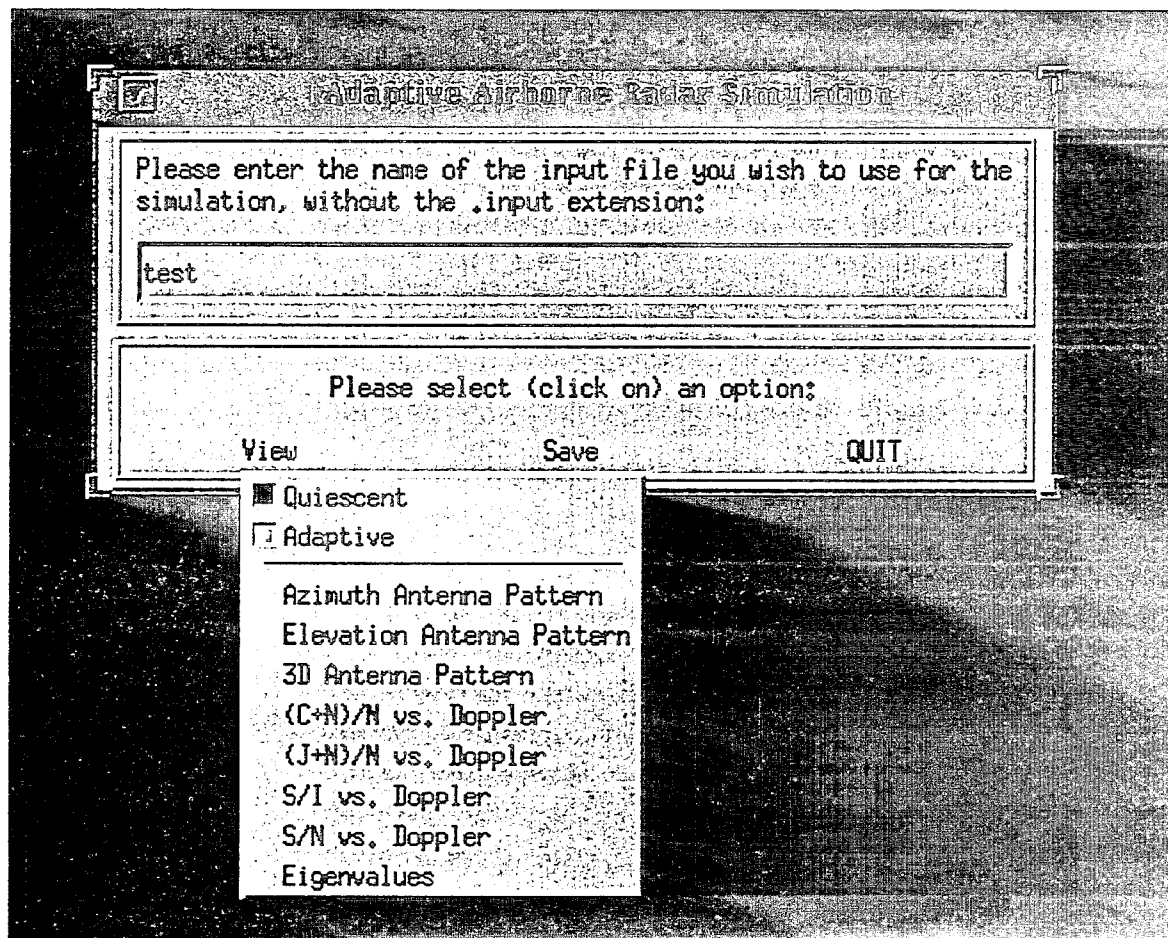


Figure 20. View Simulation Output Data Option

SECTION 5

DEMONSTRATION OF STEADY-STATE SIMULATION

The capability provided by the steady-state simulation was demonstrated by its use for the Joint Airborne Early Warning (AEW) STAP Requirements Study. Simulated output I & Q data cubes for an airborne radar with a high PRF were created from the covariance matrix of the steady-state simulation. A Cholesky decomposition is applied to the steady-state covariance matrix for each range. The lower triangular matrix that is created is multiplied by a complex Gaussian variance vector with zero mean to obtain the I & Q data samples for each range. This is repeated for each of the unambiguous ranges. The size of the data cubes was 32 elements x 256 pulses x 140 ranges (the unambiguous range interval). Because of the design of the antenna, this required a simulation with both vertical and horizontal spatial DOF in the array aperture. An example of the spectrum obtained from two data cubes created from two Monte Carlo runs for the same scenario is shown in Figure 21. The average of a large number of these spectra approaches the steady-state spectrum.

A second demonstration is based upon a MCARM experiment scenario described by the radar and environmental parameters in Table 1. The clutter-plus-noise-to-noise ratio obtained from two independent simulations of the scenario are compared to provide a basis of confidence in the steady-state adaptive simulation described in this report [5]. The other simulation, which only provides performance prediction of an airborne radar without adaptive processing and with idealized Doppler filters (no "spilling" between adjacent bins), has been compared closely with measured data. One unambiguous 75-km range obtained from the steady-state adaptive simulation is shown in Figure 22a. The performance for the same scenario obtained from the second simulation is shown in Figure 22b for two adjacent 75-km unambiguous range intervals. In Figure 22b, the antenna scanned to -14.5 degrees in azimuth and the 2000-Hz extent of the Doppler frequency spectrum is represented by 200 Doppler "bins." Also, the color scale of Figure 22b plot is more compressed than for Figure 22a. The high level of clutter signal calculated in the main beam, using both simulations, is caused by the high constant sigma model for clutter chosen for this scenario.

The adaptive suppression of received clutter is demonstrated with the same scenario using the steady-state STAP simulation. Figure 23a is a line plot of the same unadapted performance shown in Figure 22a. After two-pulse space-time adaptive filtering, the CNR is significantly reduced as shown in the line plot in Figure 23b.

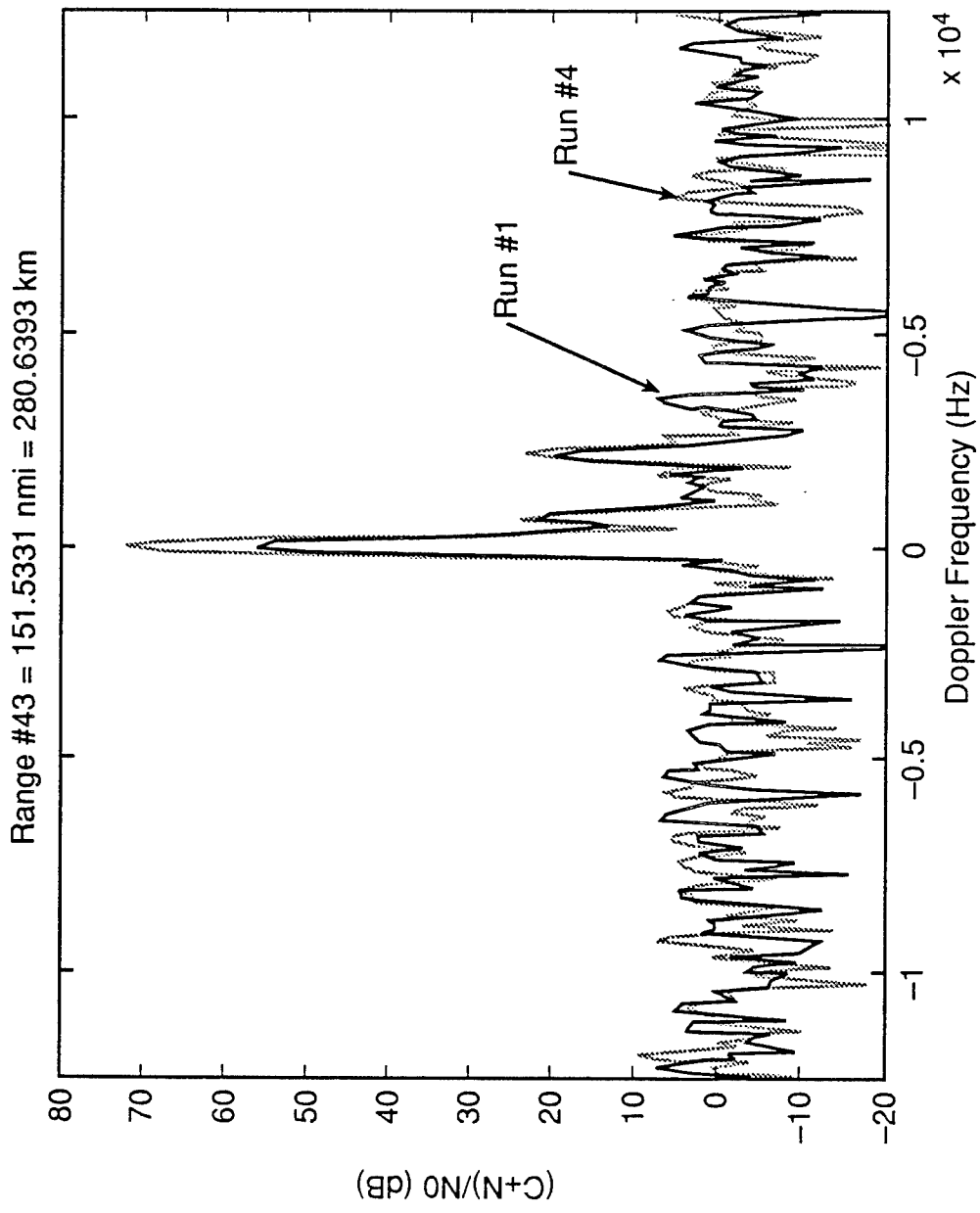


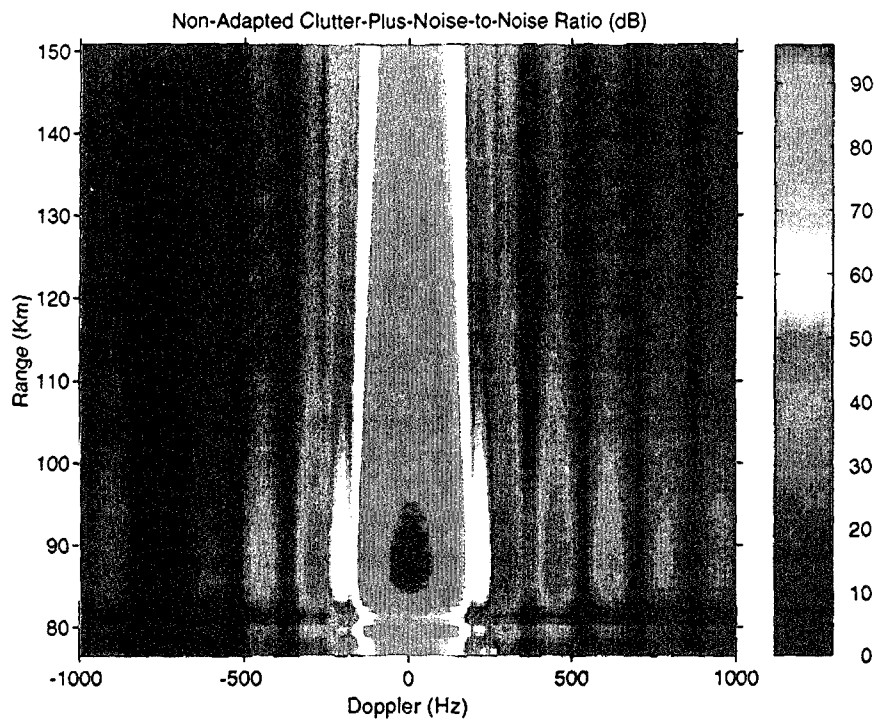
Figure 21. Examples of Finite Sample Clutter Spectra Created From Simulation With Two Spatial Dimensions of DOF

Table 1. Input Parameters for the MCARM Example

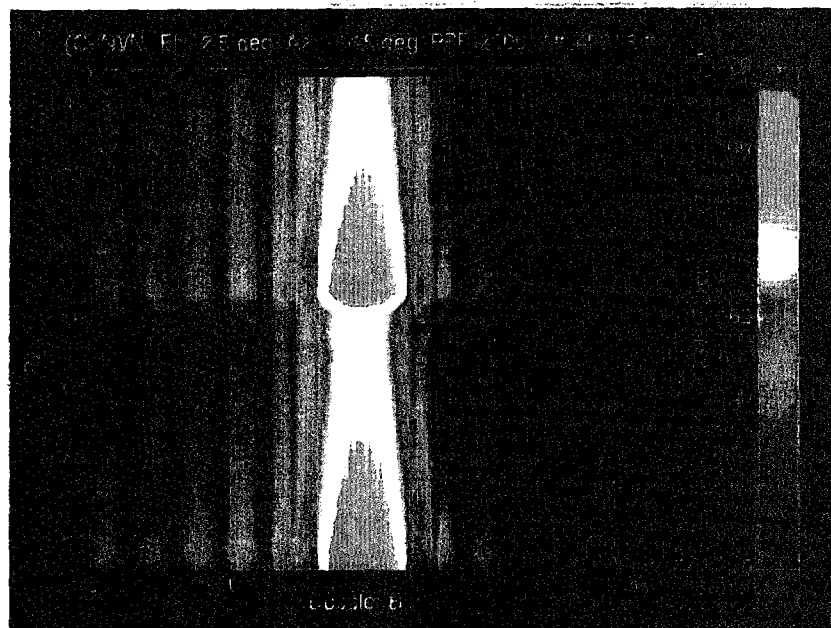
Transmit Power (kW)	14.4
Number of Antenna Columns	12
Number of Antenna Rows	8
Frequency	L-Band
PRF (Hz)	2000.0
Radar Bandwidth (MHz)	1.0
Azimuth Scan Angle (Degrees)	14.5
Elevation Scan Angle (Degrees)	2.5
Platform Altitude (Feet)	4921.5
Platform Velocity (nmi/sec)	219.7
Platform Crabbing	None
Uncompressed Pulsewidth (μ sec)	100.0
Fractional Wavelength Spacing — Columns	0.454
Fractional Wavelength Spacing — Rows	0.588
Noise Figure (dB)	2.5
System Losses	None
Additional Losses on Target Only (dB)	4.5
Atmospheric and Lens Losses	Included

Table 1. Input Parameters for the MCARM Example (Concluded)

Cancellation Ratio (dB)	60.0
Clutter Model	Constant Sigma
Mean Clutter Level, Gamma (dB)	-9.0
Internal Clutter Motion	None
Number of Near-Field Scatterers	None
Number of Coherently Integrated Outputs	200
Number of Doppler Filters	200
Doppler Weighting	100 dB Dolph-Chebyshev
Azimuth Transmit Weighting	Uniform
Elevation Transmit Weighting	Uniform
Azimuth Receive Weighting	35 dB Taylor, $\bar{N} = 4$
Elevation Receive Weighting	Uniform
Number of Receive Elevation Subarrays	2
Number of Elements Per Receive Elevation Subarray	4
Target Radar Cross-Section (m ²)	2.0
Number of Non-Adaptive Pulses Processed	1
Number of Adaptive Pulses Processed	2
Steering Vector Doppler	Half Blind Speed

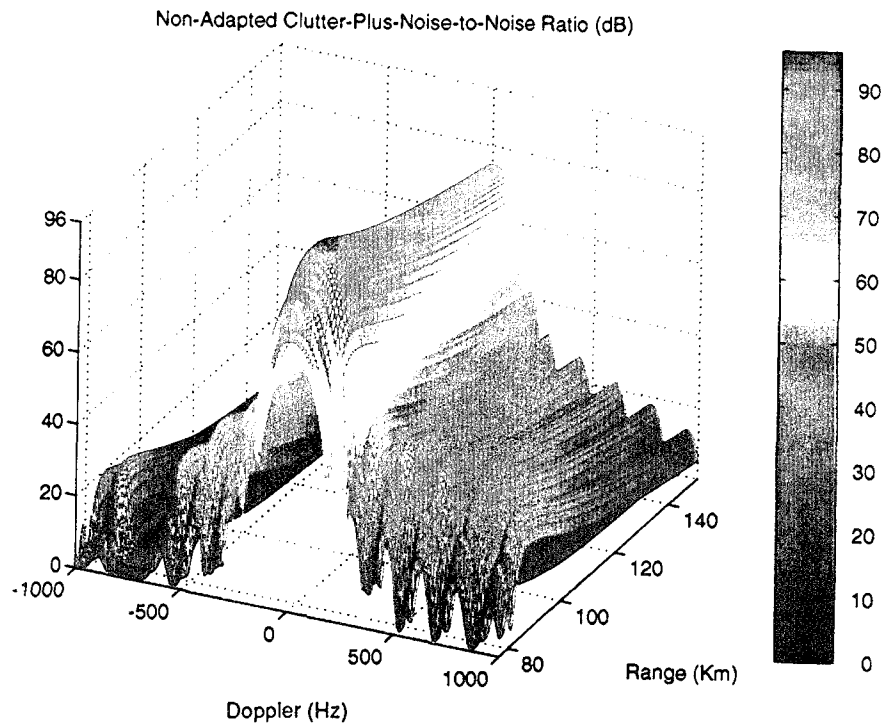


a. Steady State STP Simulation

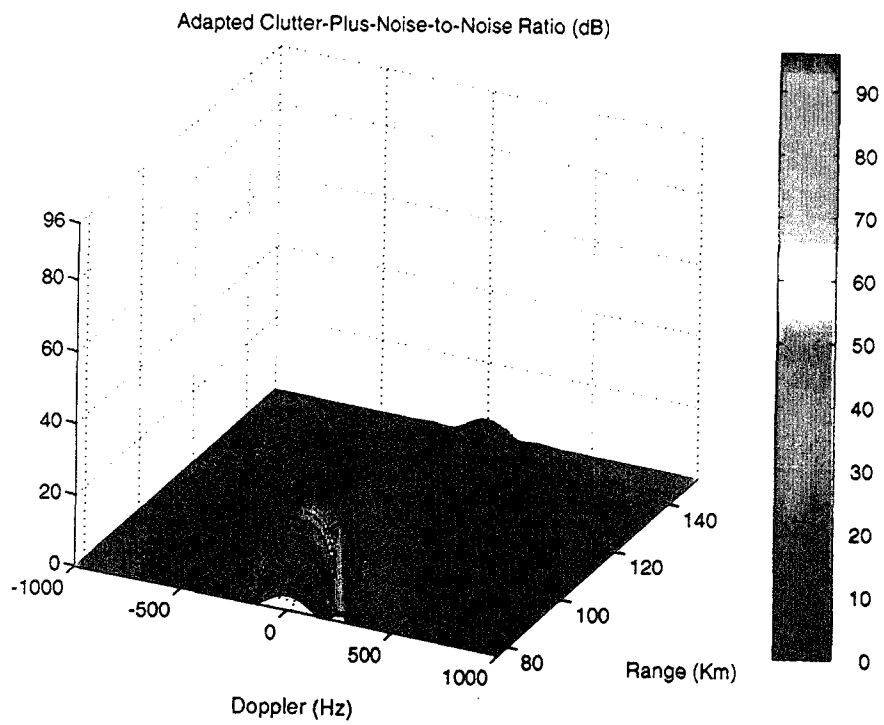


b. Reference Non-Adaptive Simulation

Figure 22. MCARM Scenario, Demonstration of Non-Adaptive Performance Using Two Independent Simulations



a. Non-Adapted Received Clutter



b. Received Clutter with 2 Pulse STP

Figure 23. MCARM Scenario, Demonstration of Clutter Reduction Using Steady-State STP Simulation

SECTION 6

APPLICATIONS FOR SIMULATION AND PROCESSING SOFTWARE

The capability and flexibility that have been added to this software will enable it to be usefully applied to many current and planned programs for predicting performance and for off-line processing of measured data. These are outlined briefly.

- MCARM experiment
 - process measured data
 - evaluate alternative processing architectures
 - effect of near-field scattering for antenna platform
 - predict performance (increase of CNR) when beam is steered toward wing
 - process measured clutter data with beam steered toward wing
 - evaluate options for processing architectures to suppress near-field scattering
 - insert near-field scattering effects into clutter data measured using free space antenna
 - predict performance of current and real-time MCARM experiments and identify beneficial data gathering scenarios
- Demonstrate increased surveillance capability of slow, small targets for AWACS radar using STAP
 - reconfigured MCARM array (8 rows x 16 columns, two to four subarrays/row, horizontal polarization) to provide more elevation DOF and fit in same radome on BAC1-11
 - model flight and scan configurations to provide "J hook" characteristics in measured clutter data
 - evaluate processing techniques based upon row outputs for suppressing clutter
 - evaluate sidelobe canceler architectures for AWACS using auxiliary radiators around periphery of array and guard channel

- ARPA mountain top data reduction
 - process measured data
 - insert effects of near-field scattering into measured data and evaluate processing techniques
 - predict performance of future airborne experiment using RSTER radar
- Rome Laboratory's Bistatic Adjunct Surveillance System (BASS)
 - predict performance with alternative STAP architectures
 - process measured or simulated I & Q data from receiving array outputs
- Predict performance of future airborne phased array radar candidates and evaluate alternative STAP architectures

SECTION 7

CONCLUSION

Enhancements have been added to our STAP steady-state simulation and processing software for an airborne phased array radar that provide more flexible models of the antenna and processing architecture and more realistic models for the simulation of the electromagnetic environment. Also, a GUI has been created that makes it simpler to control the input parameters, to examine input data files and to provide a flexible choice of output performance parameters and output formats. As a result, the simulation can be more effectively used to predict the performance of airborne radars and examine the potential benefits of using adaptive STAP with these radars. Also measured or simulated finite sample data can be processed to determine the viability of alternative processing architectures. These new features and capabilities have been demonstrated and potential applications identified.

LIST OF REFERENCES

1. Suresh Babu, B. N., and J. A. Torres, 1992, *Advanced Airborne Radar Simulation with Adaptive Antenna Techniques, Volume 1*, MTR 92B0000058V1, The MITRE Corporation, Bedford, Massachusetts.
2. Suresh Babu, B. N., and J. A. Torres, 1992, *Advanced Airborne Radar Simulation with Adaptive Antenna Techniques, Volume 2*, MTR 92B0000058V2, The MITRE Corporation, Bedford, Massachusetts.
3. Suresh Babu, B. N., and J. A. Torres, 1992, *Investigation of Some Critical Issues of Space-Time Processing (STP) Affecting Airborne Radar Performance*, MTR-11055, The MITRE Corporation, Bedford, Massachusetts.
4. Suresh Babu, B. N., and J. A. Torres, 1993, *Theory and Implementation of Equalization Filter Taps in the Advanced Airborne Radar Simulation with Adaptive Antenna Techniques*, MTR 93B0000017, The MITRE Corporation, Bedford, Massachusetts.
5. Suresh Babu, B. N., and J. A. Torres, 1994, *Enhanced Capabilities of the Advanced Airborne Radar Simulation*, MTR 94B0000109, The MITRE Corporation, Bedford, Massachusetts.
6. Barile, E. C., T. P. Guella, and D. Lamensdorf, September 1993, *Adaptive Antenna Space-Time Processing Techniques to Suppress Platform Scattered Clutter for Airborne Radar*, Symposium on Antenna Applications, Allerton Park, Illinois.
7. Lo, Y. T., and S. W. Lee (editors), 1988, *Antenna Handbook*, Chapter 20 (W. D. Burnside and R. J. Marhefka), Van Nostrand Reinhold Company, New York.
8. Zamosciany, S., 1993, *Generalized Finite Sample Space-Time Processing Simulation*, WP 92B0000359, The MITRE Corporation, Bedford, Massachusetts.
9. DiPietro, R. D., October 1992, *Extended Factored Space-Time Processing for Airborne Radar Systems*, 26th Annual Asilomar Conference on Signals Systems and Computing.
10. Sniezek, C. J., October 1994, *Graphical User Interface (GUI) for the Advanced Airborne Radar Simulation*, WP 94B0000137, The MITRE Corporation, Bedford, Massachusetts.

GLOSSARY

AEW	Airborne Early Warning
ARPA	Advanced Research Projects Agency
AWACS	Airborne Warning and Control System
BASS	Bistatic Adjunct Surveillance System
CNR	clutter-plus-noise-to-noise ratio
CPU	central processing unit
DOF	degrees of freedom
GTD	geometric theory of diffraction
GUI	graphical user interface
JNR	jammer-plus-noise-to-noise ratio
MCARM	Multichannel Airborne Radar Measurements
NECBSC	Numerical Electromagnetics Code-Basic Scattering Code
PRF	pulse repetition frequency
PRI	pulse repetition interval
RL	Rome Laboratory
SIR	signal-to-interference ratio
SNR	signal-to-noise ratio
STAP	space-time adaptive processing
STP	space-time processing
Tcl and Tk	Tool Command Language and Toolkit

MISSION
OF
ROME LABORATORY

Mission. The mission of Rome Laboratory is to advance the science and technologies of command, control, communications and intelligence and to transition them into systems to meet customer needs. To achieve this, Rome Lab:

- a. Conducts vigorous research, development and test programs in all applicable technologies;
- b. Transitions technology to current and future systems to improve operational capability, readiness, and supportability;
- c. Provides a full range of technical support to Air Force Materiel Command product centers and other Air Force organizations;
- d. Promotes transfer of technology to the private sector;
- e. Maintains leading edge technological expertise in the areas of surveillance, communications, command and control, intelligence, reliability science, electro-magnetic technology, photonics, signal processing, and computational science.

The thrust areas of technical competence include: Surveillance, Communications, Command and Control, Intelligence, Signal Processing, Computer Science and Technology, Electromagnetic Technology, Photonics and Reliability Sciences.